On the competition of laser acceleration mechanisms of electrons and ions in steep density profiles at overdense plasmas interfaces

Stefan Hüller, Anna Porzio, Anne Héron

On the competition of laser acceleration mechanisms of electrons and ions in steep density profiles at overdense plasmas interfaces

Stefan Hüller,[1] Anna Porzio,[2,1] and Anne Héron[1]
[1)] *Centre de Physique Théorique(CPHT), CNRS, Ecole Polytechnique, IP Paris, 91128 Palaiseau, France*
[2)] *LAGA, Institut Galilée, Université Paris 13, Villetaneuse, France*

The role of the density gradient in the electron acceleration process by intense laser pulses for a plasma profile with a steep interface between vacuum and a strongly overdense plasma is investigated. In a recent article (see Phys. Plasmas 26, 083107 (2019) ; see also Phys. Rev. E 84, 025401 (2011)) it has been shown that the distribution function of electrons accelerated by intense laser pulses at abrupt vacuum-plasma interfaces is of non-thermal nature in its high-energy tail due to stochastic electron acceleration. Here laser intensities in the relativistic regime are considered. Ponderomotive steepening in plasma profiles with non-zero density gradients leads to a steeper gradient in the overdense part of the interface and to the formation of an electron cloud in front of it. The latter favours collective electron motion in the underdense plasma which alters significantly the evolution of the distribution of electrons that are injected into the dense plasma. This leads eventually to heating of the electrons inside the dense plasma without the generation of a pronounced high energy tail as seen for abrupt interfaces. The different heating mechanisms have consequences on the onset of the ion motion at the rear of the target. In particular the heating of the resulting hot electron population predominant for the ion expansion evolves in time. For finite gradients the acceleration is dominated by ponderomotive effects at the laser interface and the resulting electron kinetic energy is hence limited by the oscillatory energy. For very steep interfaces an ultra-relativistic and non-thermal electron population exits the rear of the target, its influence on the ion expansion is eventually masked by the heated electron bulk. While time evolution of the hot electron population is not considered in the known analytic models, we show here that the ion dynamics can still be quite well reproduced with this model provided that the hot electron population be traced in determining its temperature and density.

24 November 2022

I. INTRODUCTION

Ultra-intense laser pulses that impinge on a dense plasma target can accelerate electrons to highly relativistic energies such that they can penetrate into a dense target. When those electrons arrive at the rear face of the dense target, rarefaction of the plasma profile[1,2] and strong charge separation effects[2,3] lead to the acceleration of the plasma ions. The ion acceleration process depends on the efficiency of the conversion of the laser energy into electron heating, and, according to models[2–9] on the temperature of the hot electron tail of the distribution. Imprint of micro structure and/or of the excitation of surface modes on the dense target surface has been investigated to improve the conversion efficiency in order to inject electrons into the dense plasma. In recent work by Héron et al.[10] it was found that a density gradient at the interface where the intense laser pulses impinges on the dense target may act favourably for conversion in electron energy. While today electron acceleration is considered in the relativistic laser intensity regime, the latter process is well known already from the regime of non-relativistic intensities, even related to wave conversion processes, both in their linear and non linear stage[11–13].

Heating of electrons is known from the 1970's via resonance absorption, mostly for the case of obliquely incident and p-polarized laser light for the case of non-relativistic intensities[11,12]. At higher intensity, and in particular when profile steepening arises, other processes come into play[13]. For the case of relativistic laser intensities, with a pre-plasma in front of the critical density, the electron acceleration has been revisited later by Kemp et al.[14], taking into account ponderomotive profile steepening and ponderomotive heating of the electrons.

In this article we focus on the production of a hot electron population and the acceleration of ultra-relativistic electrons in a steep laser-plasma interface. We furthermore examine the role of the plasma profile on the acceleration of ions at the rear of the target due to the modification electron distribution by those laser-induced electron heating. The results presented are based on particle-in-cell (PIC) simulations with the code Emi2d developed by J. C. Adam and A. Héron at CPHT, in a version with 2 dimensions in the configuration- and 3 in momentum space (2D3V). The simulation configurations are based on target of thickness between $150k_0^{-1}$ and $300k_0^{-1}$ and width of $27k_0^{-1}$. The interactions in such configurations in 2D geometry, with 3V in momentum space, are complex, with respect to both the effects along the target surface and the effects inside the dense target with return current effects and magnetic field generation[15], we concentrate here on the electron and ion motion, as well as of the fields in the direction of laser propagation, with normally incident laser light. In the majority, the results are presented in the spatial average over the dimension y perpendicular to the laser axis.

Let us, first, summarize the results from our pre-

ceding publication[16], in which we have shown that the multi-dimensional aspect is crucial for the production of energetic electrons for intense laser pulses. In this article we have shown that energetic electrons ejected from the laser-dense plasma interface into the direction of the incoming laser are subject to successive stochastic acceleration[17,18]. Stochastic acceleration is explained by the non linear motion in the standing wave field[19,20] formed by the incident and reflected light. In first approximation, this acceleration process can be simplified to 1D geometry. However, the light fields do not have a plane wave structure due to upcoming filamentation which is eventually the reason why a certain population of energetic electrons can be ejected into the vacuum region, otherwise impossible in 1D geometry[21].

While in this preceding work we have initially considered an abrupt density jump, we investigate here aspects that appear when the plasma density gradient is finite. The latter can be characterized by the electron density gradient length $L_g = (n_e/\partial_x n_e)|_{n_e=n_c}$ at critical density n_c where the plasma frequency, ω_{pe} equals the laser frequency, i.e. $\omega_0 \equiv \omega_{pe}(n_e = n_c)$. Kemp et al. in Refs. 14 and 22 underline that the physics at the interface change considerably in presence of a pre-plasma which appears intrinsically with a finite density gradient. Although ponderomotive profile steepening will limit the gradient L_g^{-1} at critical density, an underdense "foot" of electron population will form collective oscillations of those electrons in the superposed (incident and reflected) light field. As explained in what follows, only a small portion of the electrons in such a pre-plasma are energetic, such that the resulting heating process is different from stochastic acceleration.

Our article is organized as follows: in the first section, after defining the configurations of the plasma profiles used, we illustrate via phase space snap shots from PIC simulations and the resulting distribution functions the essential features of acceleration processes in comparing plasma profiles with an abrupt jump up to $100n_c$ with profile with a finite gradient $k_0 L_g$ =1 or 3. In the section on the ion acceleration at the rear of the target, we elaborate the features of the electron and ion distribution functions essential for the rarefaction of the profile. We compare furthermore the evolution ot the outgoing ion front with theoretical models, before concluding with discussions.

II. EMI2D SIMULATIONS

A. Simulation set up

We have performed simulations with the PIC code EMI2D with a laser pulse with a ramp in that reaches its maximum intensity after $\omega_0 t = 100$, keeping this maximum value until the end of the simulation. The intensity values applied correspond to normalized vector potential amplitudes a_0 [$= eE_L/(m_e\omega_0)$] = 2.8 and = 8.8,

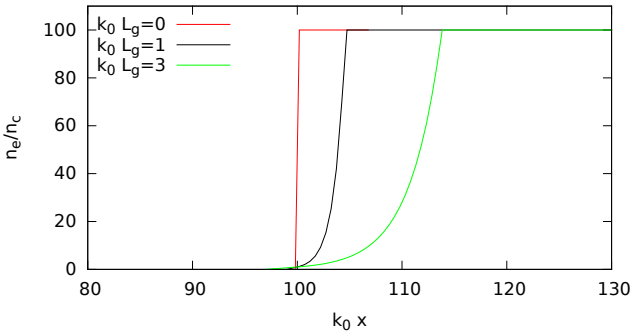

FIG. 1. Density profiles n_e/n_c as a function of x at the vacuum plasma interface for three different gradient lengths L_g at the critical density following the profile shape following Eq. (1).

as indicated in the text. The plasma interface situation around $100k_0^{-1}$ reflects the incoming laser light such that after $\omega_0 t = 200$ potentially a standing wave structure between incident and reflected light fields can form. The thickness of the target was chosen such that only fast particles can transverse the bulk, but no fields, namely between $150k_0^{-1}$ and $300k_0^{-1}$. Rarefaction on both sides remains uncoupled over the simulation duration. The width of the simulation box was chosen as $27k_0^{-1}$. The simulations were performed with mobile ions, without applying collisions, in a hydrogen plasma with an initial electron thermal speed of $v_{th,e}$ =0.03c (T_e = 230eV) and an ion/electron temperature ratio of T_i/T_e =0.1.

B. Pre-plasma formation: step profile vs. gradient

Figure 1 illustrates the front profiles of the plasma profiles chosen, with a step-like shape, up to $10n_c$ and exponentially increasing profiles between $n_e = n_c$ and $100n_c$, while a linear has been chosen for lower densities, as defined by

$$\frac{n_e(x)}{n_c} = \begin{cases} 0 & \text{for } x < x_c - L_g, \\ 1 + \frac{x-x_c}{L_g} & \text{for } x_c - L_g < x < x_c, \\ e^{(x-x_c)/L_g} & \text{for } x_c \le x < x_c + \log 100, \\ 100 & \text{for } x \ge x_c + \log 100\ , \end{cases} \tag{1}$$

with x_c denoting the position of the critical density n_c. The step-like profile corresponds hence to $L_g \to 0$.

The entire density profiles of electrons and ions (here charge $Z = 1$) are illustrated in Figs. 2 and 3, respectively, for three cases with initially different gradients, namely, $k_0 L_g = 0$ (red lines), = 1 (black), and = 3 (green), for two time instants, $\omega_0 t$ =200 (early, dashed lines) and =800. The values shown are averaged over the whole width of the second dimension y in the 2D simulation. While electron profiles are oscillatory (ondulated:

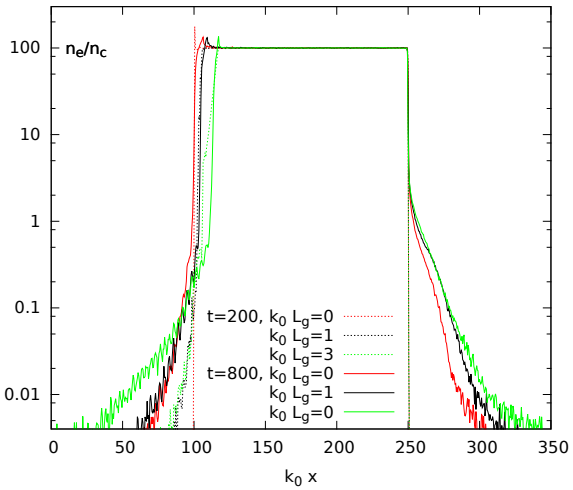

FIG. 2. Electron density profiles n_e/n_c, averaged over y, as a function of x, for two different time, $\omega_0 t$ =200 and 800, and for all three cases $k_0 L_g$ =0,1, and 3 (red, black, and green lines respectively).

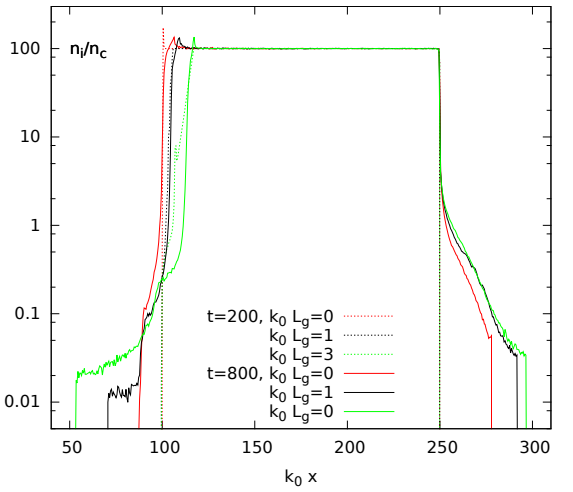

FIG. 3. Ion density profiles n_e/n_c, averaged over y, as a function of x, for two different time, $\omega_0 t$ =200 and 800, and for all three cases $k_0 L_g$ =0,1, and 3 (red, black, and green lines respectively).

front) or noisy (rear), the ion profiles show a clear front of expansion on each side.

Figures 4 and 5 illustrate how an initially step-like profile and how an exponential profile evolve with ongoing time. While the step-like profile keeps a very steep gradient around $x = x_c = 100k_0^{-1}$ with $n_e(x_c) = n_c$, a low-density foot with $n_e < 0.1n_c$ develops as pre-plasma for $x < x_c$. For the exponentially-shaped profile the low-density foot occurs at quite earlier and at higher densities. On the other hand, the initial gradient, here $L_g^{-1} = k_0/3$ steepens considerably and the position of the

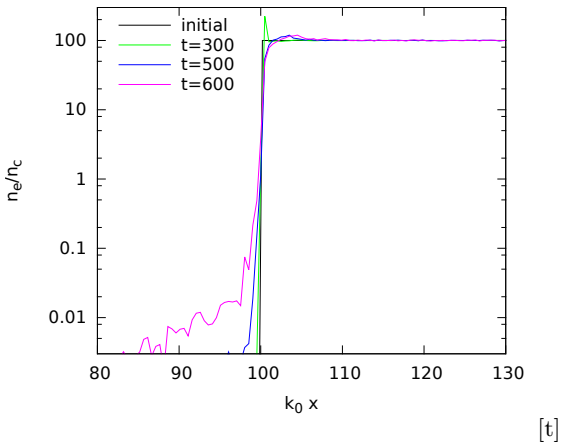

[t]

FIG. 4. Electron density profiles n_e/n_c, averaged over y, as a function of x, at the vacuum plasma interface for three different times and for the case of an abrupt density jump ($k_0 L_g$ =0) in the initial density profile. A non-negligible pre-plasma at low density ($< 0.03n_c$) forms lately

critical density is shifted towards higher values in x due to the light pressure.

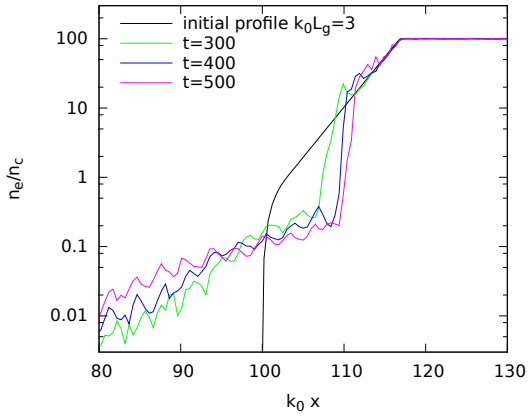

FIG. 5. Electron density profiles n_e/n_c, averaged over y, as a function of x, at the vacuum plasma interface for three different times and for the case of an initial density gradient $k_0 L_g = 3$ (black line). Around the critical density, initially at $k_0 x_c = 103$, the profiles are steepened with a typical scale length $k_0 L_{\rm steep} \simeq 0.5$. An extended pre-plasma with periodic density ripples forms in front the steepened gradient.

C. Acceleration and heating in the steep front layer

As a consequence of the different profiles and absolute electron densities in the "pre-plasma" , the electron distribution function evolves differently for the cases with a step-like profile and profiles with a finite gradient at n_c. This can be best illustrated in inspecting phase space snapshots of the electron momenta p_x versus x, as shown,

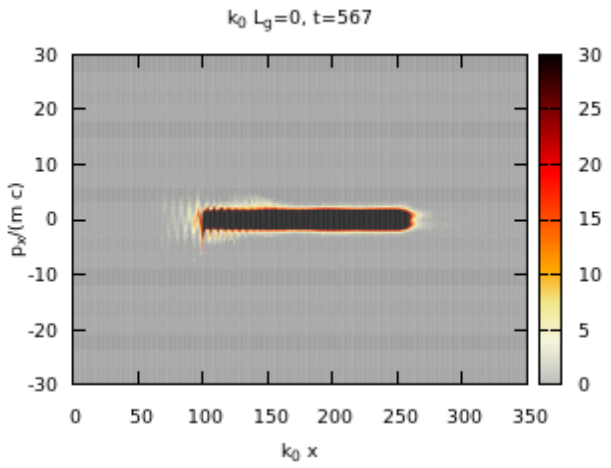

FIG. 6. Phase space contour snap shot, of the entire simulations box, taken at $\omega_0 t$ =560 for the case of an initially step-like profile with $a_0 = 2.8$.

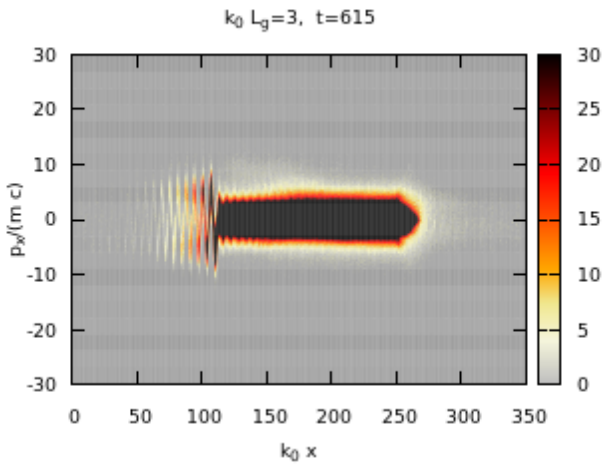

FIG. 7. Phase space contour snap shot, of the entire simulations box, taken at $\omega_0 t$ =614 for the case of an initially exponential profile ($k_0 L_g = 3$) with $a_0 = 2.8$.

respectively, in Figs. 6 and 7 for the cases of a step-like profile and a profile with gradient, here even with a steeper profile, namely $L_g = 1k_0^{-1}$. The color bars for the phase space contours are chosen with the purpose to highlight the essential physics in the front of the high density plasma bulk, the latter appearing in saturated dark colour. For both cases one can observe an ondulation in the electron phase space contours following the standing wave pattern formed by the superposition of the incident laser field and the reflected light. The number of particles, consistent with the observation concerning Figs. 4 and 5, is higher for the case with gradient.
It is remarkable that in the case of the step-like profile the ondulated contours are less filled around smaller values of $|p_x|$ and electrons are concentrated around already high (relativistic) peak values. This is a clear signature of the stochastic acceleration mechanism, identified in our previous work[16] for this configuration, and in Refs. 17, 18, and 21, for which the momenta $|p_x|$ of energetic electrons are gradually increased each time with a change in sign of p_x. For the cases with a finite density gradient, stochastic acceleration is also present, but it is practically masked by the bulk of lower energetic electrons in the pre-plasma for which the ondulation in the $p_x(x)$ contours is almost "filled up". Kemp et al.[14,22] have studied in detail the heating process for such profiles by showing that a bulk heating occurs in the layer of the gradient, attaining a width associated with ponderomotive effects. This mechanisms is however different from the one described for a thin layer[23].

D. Electron distributions in the steep front layer

The acceleration mechanisms observed in the front layer, depending on the profile gradient, have clear consequences to the electron distribution functions. To illustrate this, we have determined the distribution densities $f(p_x)$ For the case of an initially step-like profile, as illustrates figure Fig. 8, the bulk of the electron distribution widens slowly in p_x up to times $\omega_0 t$ ∼500, after which ultra-relativistic energy tails emerge, in particular for positive $p_x/m_e c$ values > 10, and later beyond $p_x/m_e c = 20$. This corresponds to what has been observed for stochastic acceleration[16].

For the case of an initially exponential profile, see Fig. 9, the widening of the bulk of the electron distribution occurs faster, while a ultra-relativistic energy tail emerges to a considerable minor degree. On the other hand, for similar times, the distributions of the case with an exponential profile produce systematically higher values in the range $|p_x| < 10$, resulting in a more efficient heating of the electron bulk.

E. Evolution of the electron distribution at the rear layer

The figures illustrating the phase spaces, Figs. 10 and 11, show the arrival of heated electron at the rear of the target, with respect to Figs. 6 and 7, respectively. The gradual heating and the arrival of ultra-relativistic particles at the rear is shown in Figs. 12-14, comparing the distribution density of the electrons $f(p_x)$ for the cases with the step-like,, Fig. 12, and exponential front profile for different times, Figs. 13 and Fig. 14. Again, as remarked in the previous section, the ultra-relativistic

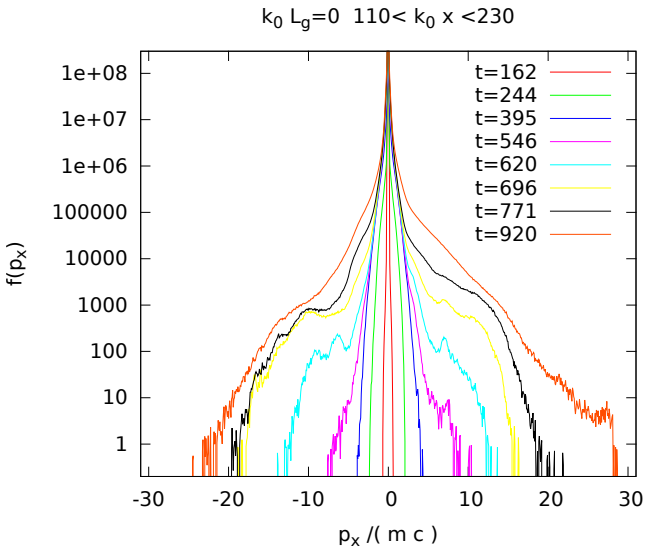

FIG. 8. Distribution density $f(p_x)$ of electrons, at different time instants (times in ω_0^{-1}), taken in the bulk of the plasma ($100< k_0x <230$), as a function of the electron momentum $p_x/(m_ec)$ for a density profile with a jump between $n_e = 0$ and $n_e = 100n_c$ at $x = x_c$ (i.e. $k_0L_g = 0$).

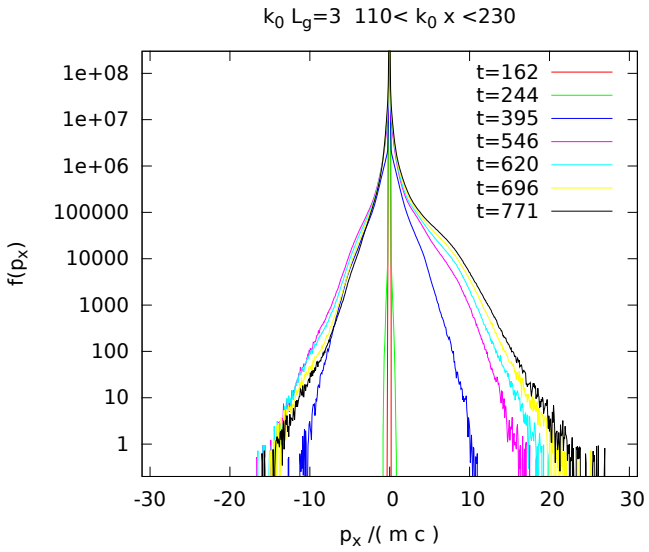

FIG. 9. Distribution density $f(p_x)$ of electrons, at different time instants (times in ω_0^{-1}), taken in the bulk of the plasma ($100< k_0x <230$), as a function of the electron momentum $p_x/(m_ec)$ for a density profile with a jump between $n_e = 0$ and $n_e = 100n_c$ at $x = x_c$ (i.e. $k_0L_g = 0$).

electron tail is more prominent for the case with a step-like front profile. Let us remark that the symmetry of the distribution is essentially forced by the electrostatic double layer recalling the not so energetic electrons after their escape from the ion bulk. This is however not true for the most energetic electrons, which could in principle leave the simulation box (before being re-introduced in order to conserve the charge). As in the situation of the front layer, for the same times, the distributions for the exponential front profile show systematically higher values in the range $|p_x| < 10$. It has the consequence that the heating is faster for the exponential profile case.

From the distribution densities $f(p_x)$ obtained via the PIC simulations, as shown in Figs. 12-14, we have determined the electron temperature over the interval of $k_0\Delta x \sim 20$ at the rear of the bulk. The fact that not too short laser pulses continue to heat the plasma from the front side, the particle distribution evolves with a tendency to reinforce the population of energetic electrons. The quantities of interest related to momenta of the electron momentum p_x, as the relativistic kinetic energy $(\bar{\gamma} - 1)m_ec^2$, could in principle be computed by integration of $f(p_x)$ via the second momentum in $p \equiv p_x/(m_ec)$, namely $(p - \bar{p})^2$ or via the kinetic energy $\gamma(p) - 1 = \sqrt{1+p^2} - 1$, by taking into account $\bar{p} = \int_{-\infty}^{\infty} f(p)p\ dp$ reflecting the local return current, being small, but non-negligible. We preferred to determine the hot electron kinetic energy in fitting each $f(p,t)$, for different times and the three cases, to a Maxwell-Jüttner distribution in the form $f_{MJ}(p) \equiv f_0 \exp(-\gamma(p)m_ec^2/\varepsilon_h)$. The values of

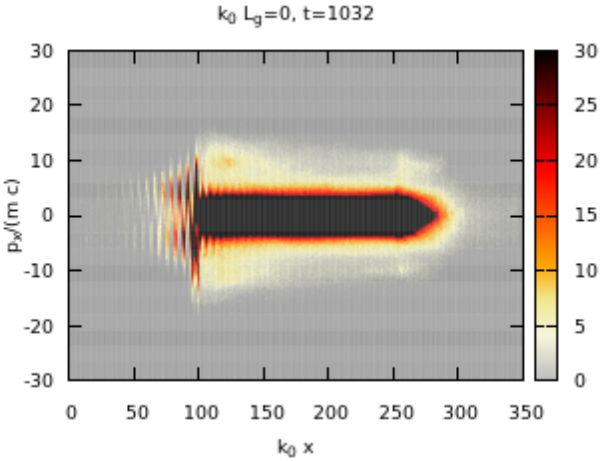

FIG. 10. Phase space contour snap shot, of the entire simulations box, taken at $\omega_0 t$ =1032 for the case of an initially step-like profile with $a_0 = 2.8$.

f_0 and ε_h were determined for each case and the available time instants.[24] The results of ε_h are reported in Tables I-III and are shown, as a function of time, in Fig. 15 for the principal hot electron population that arises besides the cold electron population, initialized with $v_{th,e} = 0.03c$ when starting the simulation. From the peak value, f_0, of each distribution, the density of the hot electron population can be obtained via integration of f_{MJ} over p, re-

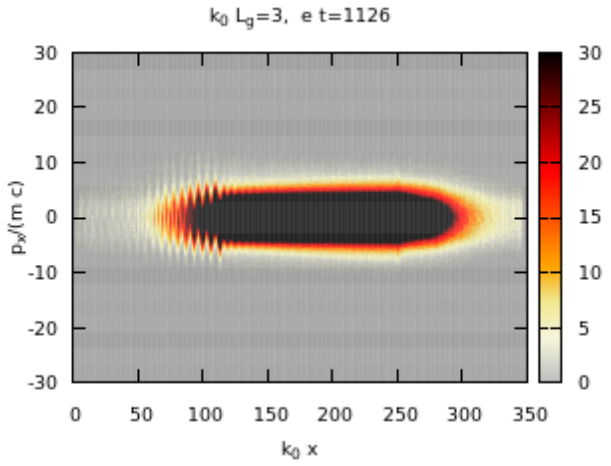

FIG. 11. Phase space contour snap shot, of the entire simulations box, taken at $\omega_0 t$ =1126 for the case of an initially exponential profile ($k_0 L_g = 3$) with $a_0 = 2.8$.

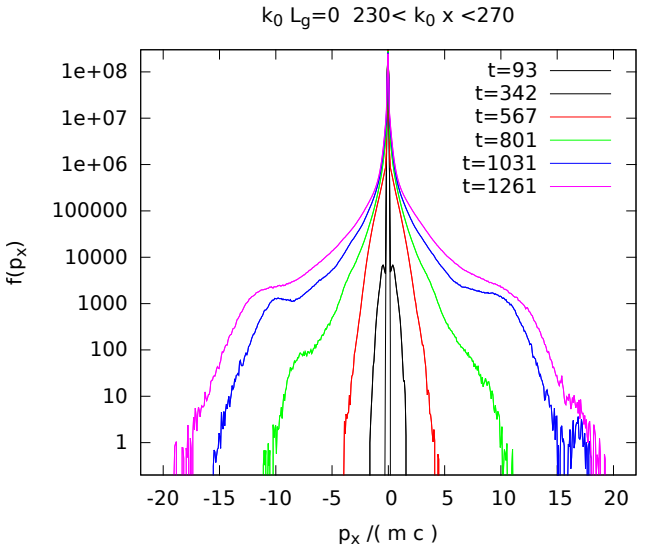

FIG. 12. Electron distribution densities $f(p_x)$ as a function of the electron momentum p_x, taken at the rear of the target for different time instants (indicated in units of ω_0^{-1}), showing the case with an abrupt jump at the front, i.e. $k_0 L_g = 0$.

sulting in $n_h = f_0 \exp(m_e c^2/\varepsilon_h) K_1(m_e c^2/\varepsilon_h)$. In Tabs. I-III these values are reported with respect to the plasma bulk density ($n_0 = 100 n_c$). In particular for the case of a step-like front profile, also a secondary ultra-relativistic population comes up after a transient period, also listed in the Table I. It should, however, be mentioned that the distributions for the case with the step-like profile have a clear cut-off at high $p_x (> 10 m_e c)$ values, see Figs. 8 and 12. For this case a fit to a thermal-type distribution,

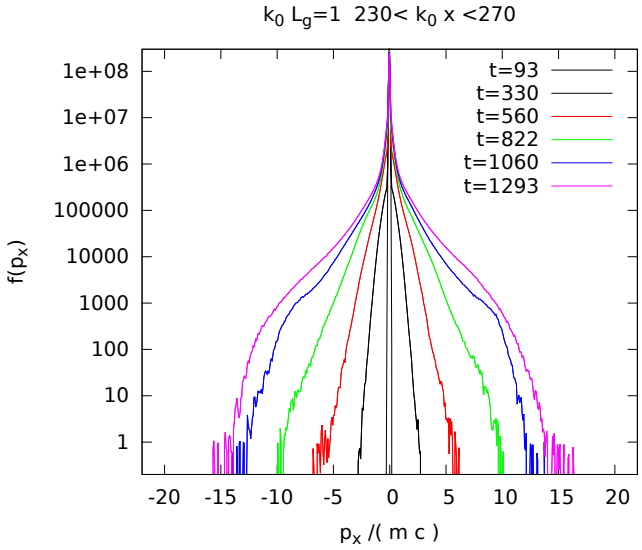

FIG. 13. As in Fig. 12, electron distribution densities $f(p_x)$ as a function of the electron momentum p_x, taken at the rear of the target for different time instants, showing the case with $k_0 L_g = 1$.

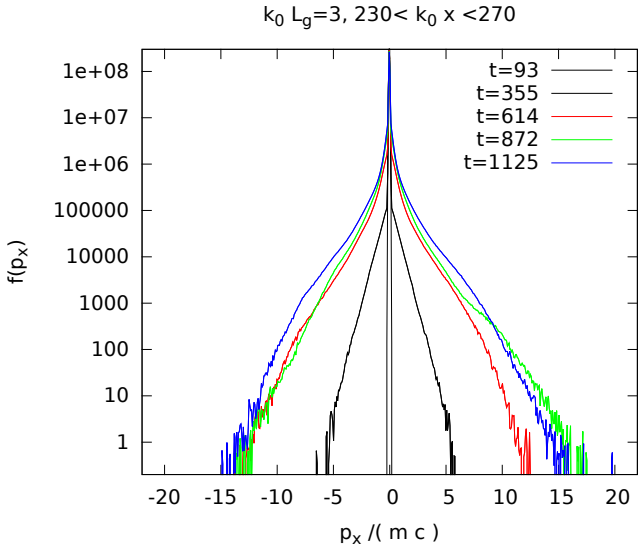

FIG. 14. As in Fig. 12 and 13, electron distribution densities $f(p_x)$ as a function of the electron momentum p_x, taken at the rear of the target for different time instants, showing the case with $k_0 L_g = 3$.

to which Maxwell-Jüttner belongs, is questionable. However, for a limited interval in p_x a fit to Maxwell-Jüttner can be found, and the corresponding ε_h values is reported $\varepsilon_{h,2}$. The extension (width in p_x) of the distributions in p_x diminishes naturally from the front to the rear of the plasma profile, due to multi-dimensional diffusion effects in phase space.

time (ω_0^{-1})	$\varepsilon_h/(m_ec^2)$	n_h/n_0	$\varepsilon_{h,2}/(m_ec^2)$	$n_{h,2}/n_0$
342	0.1	$5.6\ 10^{-4}$		
567	0.25	$3.7\ 10^{-4}$		
801	0.7	$1.8\ 10^{-2}$	1.3	$3\ 10^{-5}$
1032	1.3	$1.9\ 10^{-2}$	7.	$1.7\ 10^{-5}$

TABLE I. Case with $k_0L_g = 0$: hot electron kinetic energy and the corresponding hot electron density deduced from the distributions at the rear of the plasma bulk, shown in Fig.12, by fitting a Maxwell-Jüttner distribution. At later times an ultra-relativistic hot electron component with $\varepsilon_{h,2}$ appears, however with a cutoff at high $p_x/(m_ec) > 15$ values.

time (ω_0^{-1})	$\varepsilon_h/(m_ec^2)$	n_h/n_0	$\varepsilon_{h,2}/(m_ec^2)$	$n_{h,2}/n_0$
338	0.14	$1.3\ 10^{-2}$		
560	.35	$4.6\ 10^{-2}$		
822	0.7	$3.5\ 10^{-2}$		
1032	1.1	$3.6\ 10^{-2}$	2.	$1.3\ 10^{-4}$

TABLE II. Case with $k_0L_g = 1$: hot electron kinetic energy and the corresponding hot electron density deduced from the distributions, shown in Fig. 13, by fitting a Maxwell-Jüttner distribution. At later times an ultra-relativistic electron component with $\varepsilon_{h,2}$ appears, with, however with a cutoff at high $p_x/(m_ec) > 15$ values.

In a general manner, the distributions, as shown in Figs. 8-9 and Fig.12-14, show clearly that the electron heating mechanisms for the step-like profile is different from profiles with an already developed gradient. With gradients, the electron "bulk" is heated with an increasing effective temperature $k_BT_h \sim \varepsilon_h$, while for the step-like case this type of heating occurs only after the retarded formation of a pre-plasma. The latter depends also on multi-dimensional effects. In the step-like profile the acceleration of relativistic electrons, ejected due to multi-dimensional effects from the vacuum-plasma interface, and described in Refs.[16–18,21], is clearly visible. The

time (ω_0^{-1})	$\varepsilon_h/(m_ec^2)$	n_h/n_0	$\varepsilon_{h,2}/(m_ec^2)$	$n_{h,2}/n_0$
93	0.031	0.2		
355	0.45	$3.3\ 10^{-3}$		
615	1.1	$6.0\ 10^{-2}$		
872	1.1	$2.4\ 10^{-2}$		
1126	1.2	$3.8\ 10^{-3}$		

TABLE III. Case with $k_0L_g = 3$: hot electron kinetic energy and the corresponding hot electron density deduced from the distributions, shown in Fig. 14, by fitting a Maxwell-Jüttner distribution. No significant ultra-relativistic electron component appears in the considered time window.

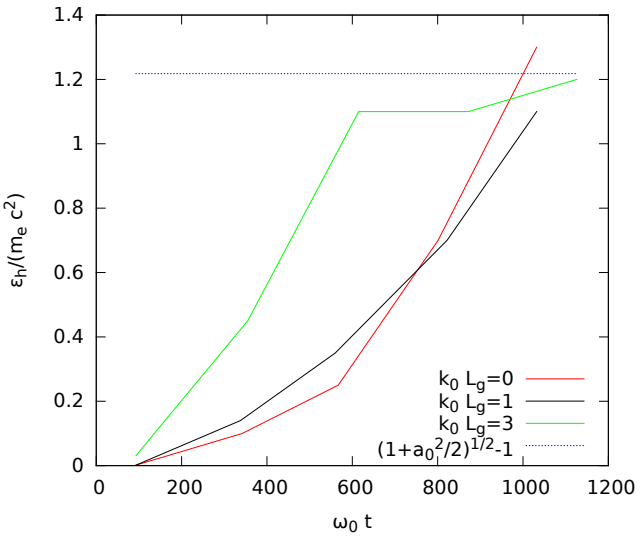

FIG. 15. Hot electron kinetic energy, $\varepsilon_h/(m_ec^2)$, as a function of time, deduced from the electron distribution densities $f(p_x)$ at the rear of the plasma bulk ($230 < k_0x < 270$), in time steps as indicated in the Tables I,II,III. Values have been obtained by fitting a Maxwell-Jüttner-type distribution to the dominating hot electron component for the 3 cases with different density gradients at the front, i.e. with a step-like profile at the front (red lines), and gradients $k_0L_g = 1$ and 3 (black and green, respectively). The dashed line shows the hot electron kinetic energy expected by ponderomotive heating according to Wilks[14,25], here $\sim 1.2m_ec^2$.

phase space plot in Fig. 10 also shows that the arrival of ultra-relativistic electrons in bunches, which is therefore not necessarily continuous in time. The formation process of ultra-relativistic electrons, due to stochastic heating in the front part, may still be present with developed gradients but it is masked by the dominant heating of the electron bulk.

Furthermore, from Fig. 15 there is strong evidence of ponderomotive type heating, as developed in Ref. 14 and 25, for the case with the longest gradient, $k_0L_g = 3$, for which the hot electron distribution tends to saturate for kinetic energy values $\varepsilon_h \to (1 + a_0^2/2)^{1/2} - 1$, here $1.2m_ec^2$. In particular for the case with the step-like profile, the distribution widens beyond this limit due to the formation of an ultra-relativistic tail.

F. Expansion of the ion and electron profiles at the rear layer

The values for the hot electron temperature are useful for models that describe the hydrodynamic expansion of the ion density profile at the rear of the plasma target. The ion front that forms and moves away from the rear face of the plasma corresponds then to effective ion acceleration, and is therefore of potential interest for applications (such as proton diagnostics).

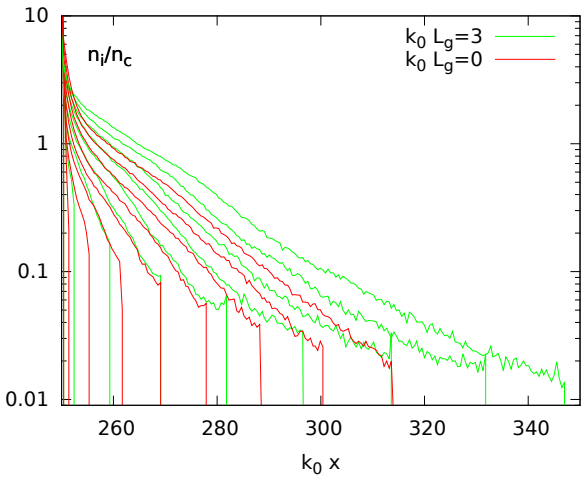

FIG. 16. The ion density profile at the rear of the target for different time instants (from $\omega_0 t$ =200 to 1100 in steps of $\omega_0 t$ =100), showing a comparison between the two cases with an abrupt jump at the front (red lines), and a gradient $k_0 L_g = 3k_0$ (green lines).

Models have been developed for planar expansion, normal to the rear face in x direction. In the context of laser-plasma interaction the assumption of an isothermal equation of state for the electrons is generally a good approximation, and for this reason most of the studies are based on an isothermal law for the electron dynamics[2,3,26–28] on the slow, ionic time scale.

Those models assume the formation of 'cold (co)' and 'hot (h)' populations characterized by their temperatures T_{co}, T_h and densities n_{co}, n_h, respectively, fulfilling $n_i \equiv n_{co}\exp(e\varphi/k_B T_{co}) + n_h \exp(e\varphi/k_B T_h)$, with k_B denoting the Boltzmann constant. In a similar manner, also the rarefaction for the adiabatic case has been considered[29,30].

Of principal interest in the case of ongoing heating of the plasma slab by the laser light at the front vacuum (pre-plasma)- dense plasma interface, is the hot electron population which develops an extended cloud at the rear, and which governs the motion of an ion front[4,27,28].

For the isothermal case in a semi-finite plasma slab the rarefaction can be considered to follow a similarity law[31] such that the spatial coordinate x and time t can be combined to a single similarity variable $x/(c_s t) \to \xi + const$ in the set of hydro-dynamic equations for continuity and momentum, with c_s denoting the sound speed of the plasma, $c_s \equiv (Zk_B T/m_i)^{1/2}$, in which Z is the ion charge. For the ion density with an exponential law, it follows then for advanced times ($c_s t \gg v_{th,e}/\omega_{pe,0}$)

$$n_i(x,t) = n_0 \exp\{-(x-x_r)/(c_s t) - 1\} \ , \qquad (2)$$

with $\xi \equiv (x-x_r)/(c_s t)$, and x_r denoting the position of the rear face of the plasma at $t = 0$. For what concerns the ion front motion, the plasma temperature T is dominated by the hot electron component $k_B T_h \sim \varepsilon_h$. The resulting ion velocity is given by $v(x,t) = (x-x_r)/t + c_s$. The balance between the electron pressure and the electrostatic field, $eE_x = -(1/n_e)\partial_x(n_e k_B T)$, keeps quasi-neutrality. From Eq. (2) it follows for an isothermal plasma[4]

$$E_{x,s} = k_B T_h/(ec_s t) = E_0/(\omega_{pi} t) \ , \qquad (3)$$

with ω_{pi} as the ion plasma frequency (in the unperturbed plasma) of the hot electron component, and $E_0 \equiv (n_0 k_B T/\epsilon_0)^{1/2}$. For advanced expansion, quasi-neutrality can no longer be maintained in the lower shelf. This occurs when in the plasma profile $c_s t$ equals the local Debye length.[4,31]

This process has been extensively studied, also with better precision concerning the expression for the ion front. These models assume the (hot) electron temperature as an initial value, but do not consider that the heating is maintained from the front side. A more precise expression of the evolution of the electric field at the front, even for early times, has been given in Ref. 4,

$$E_{x,f} = \frac{2E_0}{\sqrt{2e + \omega_{pi}^2 (t-t_r)^2}} \text{ with } t \geq t_r, \qquad (4)$$

with a reference time t_r, discussed later. From this expression follows also the ion front motion in time for which v_f and x_f mark the front of the ion profile, beyond and electron cloud has formed. Both v_f and x_f result by simple integration of the equation of motion

$$\frac{dv_f}{dt} = \frac{Z}{m_i} E_{x,f} \quad \text{and} \quad \frac{dx_f}{dt} = v_f \ . \qquad (5)$$

Figure 16 shows the profile of the ion density at the rear of the plasma profile, situated at $x_r = 250 k_0^{-1}$, for a series of time instants, and for both cases, step-like (red lines) and exponential (green with $k_0 L_g = 3$). The profiles exhibit a clear ion front that decreases in density. The electron profiles, not shown here follow essentially the part almost up to the front, while their profiles are naturally extended to higher x-values without a sharp front due to the large diffusion of electron energies. From the ion profiles one can deduce that there is a temporal delay between both cases. This is confirmed in the curves of Figure 18 for the time evolution of the ion fronts, deduced from the values in Fig. 16 for all three cases (again red for step-like, black and green for exponential, $k_0 L_g = 1$ and 3, respectively). In spite of the difference of the distribution functions, apart from the time delay, the behaviour are very similar, except that the case with the weakest gradient, $k_0 L_g = 3$, the acceleration of the front is faster, apparently due to the faster onset of the "bulk" hot electron population. From the speed of the ion front evolution, shown in Fig. 19, one can deduce the ion speed and the corresponding ion energy of the ions in the front. The values, for both cases, reach eventually $v_f/c \sim 0.16 \ldots 0.18$ which corresponds to ion (here proton) energies in the range of 12-15 MeV.

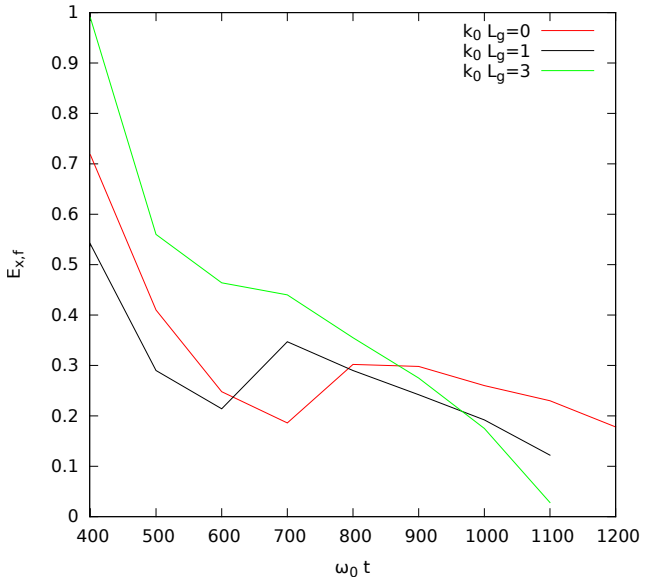

FIG. 17. Time evolution of the (normalized) electric field $eE_{x,f}/(m_e\omega_0 c)$ at the ion front position behind the target as a function of time (in steps of $100\omega_0^{-1}$), showing a comparison between the three cases with an abrupt jump at the front (red lines), and gradients k_0L_g =1 and 3 (black and green lines).

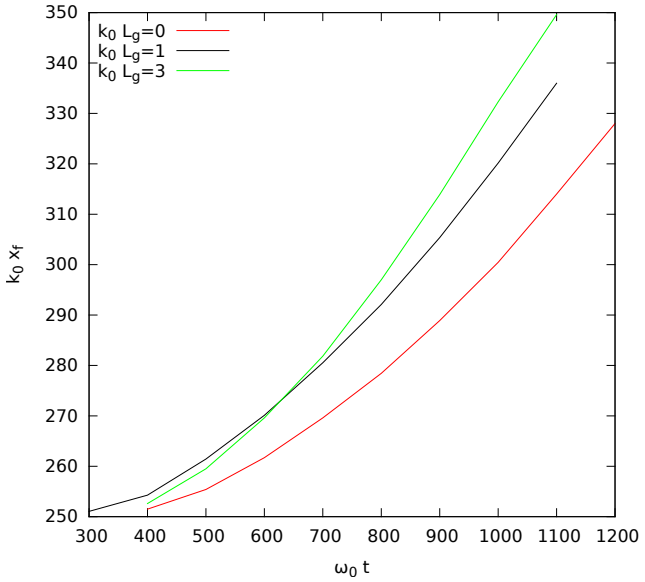

FIG. 18. Time evolution of the ion front position x_f behind the target as a function of time, showing a comparison between the three cases with an abrupt jump at the front (red lines), and gradients k_0L_g =1 and 3 (black and green lines).

It is of interest to examine the validity of Mora's model[4] for the case when the temperature and the density of the hot electron population evolve, as in the case of not too short laser pulses, as in our simulations. The expression for the electric field $E_{x,f}$ at the front in Eq. (4) depends on the initial electric field value E_0 which itself is a function of the density and the temperature of the electron population considered, n_h and ε_h, $E_0 \equiv (n_h\varepsilon_h/\epsilon_0)^{1/2}$; the ion plasma frequency depends on n_h/Z, i.e. $\omega_{pi} \equiv [n_h e^2/(Z\epsilon_0 m_i)]^{1/2}$. From the values of n_h and ε_h in the Tables I,II, and III we have computed the time evolution of $E_{x,f}$ via Eq. (4) in assuming each reference time as the time for which we knew the distribution[24]. The result of the comparison between the simulation cases with different gradients, $k_0L_g = 0$, $= 1$, and $= 3$ with the model Eq. (4) is shown in Figs. 20, 21, and 22, respectively. Several curves in blue colour correspond to the the different values as listed in Tables I,II, and III. For each case and curve, the values of the parameters E_0 and $\omega_{p,i}$ were kept constant. This method, instead of considering a smooth evolution of both parameters (with $\int_{t_r}^{t} \omega_{p,i}(t')dt'$ instead of $\omega_{p,i}(t-t_r)$) seemed to be more appropriate due to the relatively abrupt changes of $E_{x,f}$ seen in Fig. 17 for at least the cases with $k_0L_g = 0$ and $= 1$. Within the uncertainty of the values of ε_h and n_h determined from the distributions and listed in the Tables, the agreement of the temporal descent by comparing the simulation results with the dependence $\propto 1/(t-t_r)$ expected from Eqs. (4) and (3) is satisfactory in the time interval $\omega_0 t$ =400 ... 700 . The values of the reference

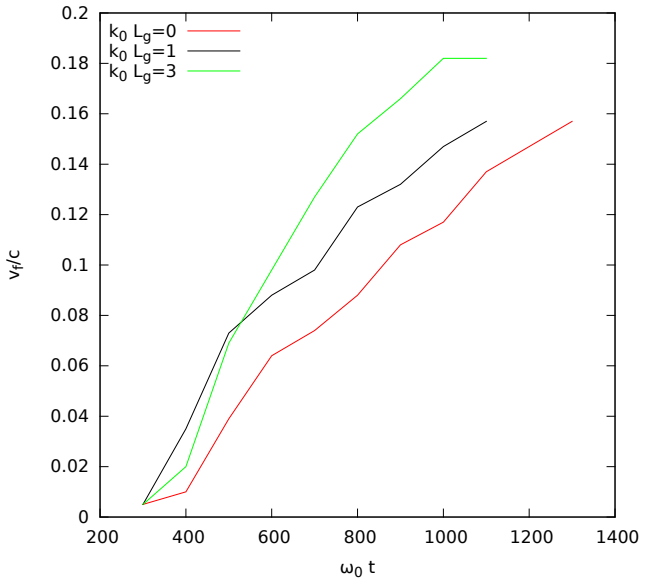

FIG. 19. Time evolution of the ion front velocity v_f behind the target as a function of time, showing a comparison between the three cases with an abrupt jump at the front (red line), and gradients k_0L_g =1 and 3 (black and green lines).

times t_r had to be chosen with care ($\omega_0 t_r$ >250) with respect to the output[24] times of phase space values and the resulting distribution densities $f(p_x, t)$. At advanced times, say for $\omega_0 t$ >600, the onset of hotter electron populations seems to re-initialises both E_0 and $\omega_{p,i}$ which is visible both in the simulations and in the model.

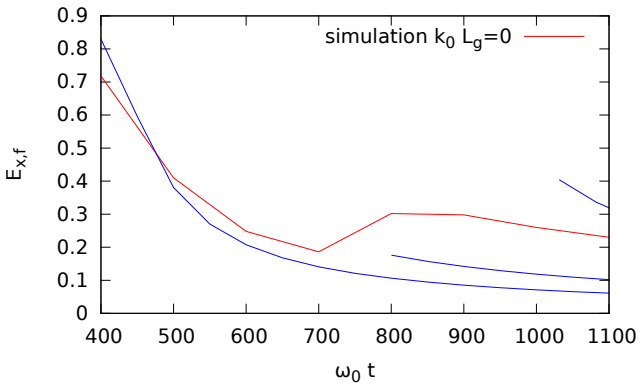

FIG. 20. Time evolution of electric field $E_{x,f}$ at the ion front, case $k_0 L_g = 0$, showing a comparison between the simulation result Fig. 17 and the analytical expression Eq. (3) starting with the E_0- and n_h- values listed in Table I with time delay (blue) lines.

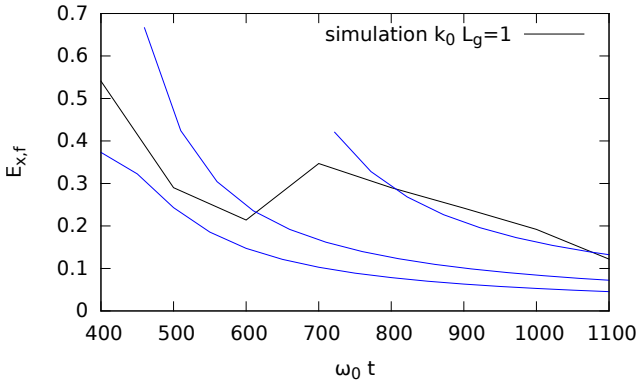

FIG. 21. Time evolution of electric field at the ion front, case $k_0 L_g = 1$, showing a comparison between the simulation result Fig. 17 and the analytical expression Eq. (3) starting with the E_0- and n_h- values listed in Table II with time delay (blue) lines.

III. DISCUSSION AND CONCLUSIONS

We have examined the acceleration of electrons and ions by laser interaction with a dense plasma with steep interfaces where the laser beam impinges on the plasma target. In particular we have studied the sensibility of electron acceleration and heating mechanisms on the gradient of a pre-formed plasma, in focusing on the dynamics normal to direction of incidence. Finite gradients may originate from pre-formed plasma by a long time-scale foot ('pièdestal') of a short laser pulse with insufficient contrast, by a preceding heater beam, or by disintegration of a pre-imprinted surface structure of specially prepared target plasmas, in spite of possible profile steepening.

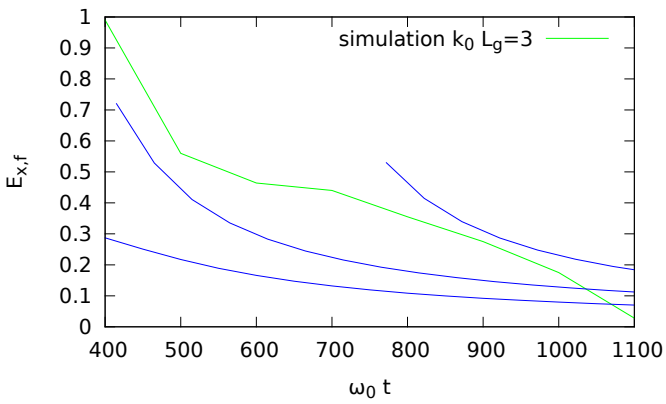

FIG. 22. Time evolution of electric field at the ion front, case $k_0 L_g = 3$, showing a comparison between the simulation result Fig. 17 and the analytical expression Eq. (3) starting with the E_0- and n_h- values listed in Table III with time delay (blue) lines. The value at early time, $\omega_0 t = 93$ in Table III corresponding to the lower line.

2D aspects in the simulations

Our simulations have been carried out with the particle-in-cell code EMI2D in 2 spatial and 3 dimensions in velocity. Most of our shown results focus on the motion in the direction of the incoming laser light. It is however important to mention that the motion across the laser propagation is important. Simulations in only 1D cannot show the essential mechanisms for acceleration because the action of the laser ponderomotive potential blocks the motion in this only direction. In 2D or 3D the shape of the electromagnetic fields become modulated due to self-focusing/filamentation. We have limited our study to an initially plane wave field, ignoring the transversal spatial shape of a focused beam, that eventually may lead to hole boring. We believe, however, that focusing and hole boring effects introduce additional parameters that do not help to find a better interpretation at this stage.

Alternative choices of parameters

We have also carried out simulations at higher laser intensity, and different sizes of the plasma. The cases shown here for the reference parameters with $a_0 = 2.8$ and the chosen plasma size, are quite representative for the obtained results. For the cases with $a_0 = 2.8$, the resulting ion front motion attains eventually proton energies of 12-15MeV.

Finite shorter pulse duration

As mentioned above, the duration of our simulations was up to 200-250 laser oscillation cycles, assuming constant laser intensity after a ramp in time. It should be remarked that the physics of the acceleration processes is considerably different as long as the laser pulse dura-

tion does not allow, as e.g. in Ref. 8, the formation of a sufficiently extended standing wave structure due to the superposition of the incident and reflected light in front of the plasma.

Concluding remarks

Although we have considered steep gradients from $k_0 L_g = 0$ to $= 3$, the mechanisms in play prove to change already in this range of L_g with respect to the electron dynamics in the incident and reflected laser-light fields in front of the plasma. Ponderomotive profile steepening stabilize the profiles, but only in the vicinity of the critical density. For those gradients, the motion of electrons, once ejected from the steep gradient interface, is dominated by the standing wave structure of the light fields due to still strong reflection. For step-like profiles, the acceleration of relativistic electrons by stochastic motion in the standing wave structure is important. Such electrons can then propagate through the dense plasma without that their motion is too much affected (depending on the target thickness). While this process may still be present for finite gradients, the ponderomotive-type acceleration of the bulk of electrons becomes predominant, leading to a heating of the electron bulk, subsequently all over the plasma. The fact that the distribution of those electrons has a close-to-thermal shape, the 'hot' electron cloud arriving at the rear of the plasma is predominant for the expansion there. This leads also to the well-known expansion of ions, which occurs in the form of an ion front and which can attain supra-thermal speeds that eventually offer interesting technological applications, such as proton radiography and for medical therapies. The understanding of the dynamics of the ion front is therefore an important goal.

We have therefore examined our simulations results with respect to analytical models in which hot electron populations with fixed density and temperature are considered. In our simulations over time intervals of $\omega_0 t$ up 1300, hence roughly 200 oscillation cycles, i.e. up to typically $500 fs$, both the temperature and the density of hot electrons evolve, and mostly increase. Analytical models for the ion front expansion may still be used to model the resulting ion front motion and the resulting energy, provided that the temperature and the relative concentration of them in the rear of the plasma bulk may be traced in their evolution.

ACKNOWLEDGMENTS

We would like to thank Patrick Mora for helpful discussions.

[1] L. M. Wickens, J. E. Allen, and P. T. Rumsby, Phys. Rev. Lett. **41**, 243 (1978).
[2] M. A. True, J. R. Albritton, and E. A. Williams, Physics of Fluids **24**, 1885 (1981).
[3] J. E. Crow, P. L. Auer, and J. E. Allen, Journal of Plasma Physics **14**, 65–76 (1975).
[4] P. Mora, Phys. Rev. Lett. **90**, 185002 (2003).
[5] A. Gurevich, D. Anderson, and H. Wilhelmsson, Phys. Rev. Lett. **42**, 769 (1979).
[6] V. F. Kovalev, V. Y. Bychenkov, and V. T. Tikhonchuk, Journal of Experimental and Theoretical Physics **95**, 226 (2002).
[7] V. F. Kovalev and V. Y. Bychenkov, Phys. Rev. Lett. **90**, 185004 (2003).
[8] V. Y. Bychenkov, V. N. Novikov, D. Batani, V. T. Tikhonchuk, and S. G. Bochkarev, Physics of Plasmas **11**, 3242 (2004), https://doi.org/10.1063/1.1738649.
[9] V. T. Tikhonchuk, A. A. Andreev, S. G. Bochkarev, and V. Y. Bychenkov, Plasma Physics and Controlled Fusion **47**, B869 (2005).
[10] A. Héron, J. C. Adam, and P. Mora, Physics of Plasmas **27**, 013103 (2020), https://doi.org/10.1063/1.5127164.
[11] J. S. DeGroot and J. E. Tull, The Physics of Fluids **18**, 672 (1975), https://aip.scitation.org/doi/pdf/10.1063/1.861216.
[12] B. Bezzerides, S. J. Gitomer, and D. W. Forslund, Phys. Rev. Lett. **44**, 651 (1980).
[13] F. Brunel, Phys. Rev. Lett. **59**, 52 (1987).
[14] A. J. Kemp, Y. Sentoku, and M. Tabak, Phys. Rev. E **79**, 066406 (2009).
[15] C. Thaury, P. Mora, A. Héron, and J. C. Adam, Phys. Rev. E **82**, 016408 (2010).
[16] S. Hüller, A. Porzio, J.-C. Adam, and A. Héron, Physics of Plasmas **26**, 083107 (2019), https://doi.org/10.1063/1.5111934.
[17] Z.-M. Sheng, K. Mima, Y. Sentoku, M. S. Jovanović, T. Taguchi, J. Zhang, and J. Meyer-ter Vehn, Phys. Rev. Lett. **88**, 055004 (2002).
[18] Z.-M. Sheng, K. Mima, J. Zhang, and J. Meyer-ter Vehn, Phys. Rev. E **69**, 016407 (2004).
[19] D. F. Escande and F. Doveil, Journal of Statistical Physics **26**, 257 (1981).
[20] G. Schmidt, Comments Plasma Phys. Controlled Fusion **7**, 87 (1982).
[21] J. May, J. Tonge, F. Fiuza, R. A. Fonseca, L. O. Silva, C. Ren, and W. B. Mori, Phys. Rev. E **84**, 025401 (2011).
[22] R. Mishra, Y. Sentoku, and A. J. Kemp, Physics of Plasmas **16**, 112704 (2009), https://doi.org/10.1063/1.3249691.
[23] S. V. Bulanov, A. Yogo, T. Z. Esirkepov, J. K. Koga, S. S. Bulanov, K. Kondo, and M. Kando, Physics of Plasmas **22**, 063108 (2015), https://doi.org/10.1063/1.4922679.
[24] Phase space output in the simulations was not as regular as field output due to the reconstruction of the phase space from numerous processors of massively parallel computing.
[25] S. C. Wilks, Physics of Fluids B: Plasma Physics **5**, 2603 (1993), https://doi.org/10.1063/1.860697.
[26] J. S. Pearlman and R. L. Morse, Phys. Rev. Lett. **40**, 1652 (1978).
[27] A. Diaw and P. Mora, Phys. Rev. E **84**, 036402 (2011).
[28] A. Diaw and P. Mora, Phys. Rev. E **86**, 026403 (2012).
[29] T. Kiefer and T. Schlegel, Physics of Plasmas **19**, 102101 (2012), https://doi.org/10.1063/1.4754863.
[30] C. Thaury, P. Mora, J. C. Adam, and A. Héron, Physics of Plasmas **16**, 093104 (2009), https://doi.org/10.1063/1.3206940.
[31] P. Mora and R. Pellat, The Physics of Fluids **22**, 2300 (1979), https://aip.scitation.org/doi/pdf/10.1063/1.862541.